A DC–DC Boost Converter With Variation-Tolerant MPPT Technique and Efficient ZCS Circuit for Thermoelectric Energy Harvesting Applications

Jungmoon Kim, *Student Member, IEEE*, and Chulwoo Kim, *Senior Member, IEEE*

***Abstract*—This paper presents a dc–dc boost converter with the maximum power point tracking (MPPT) technique for thermoelectric energy harvesting applications. The technique realizes variation tolerance by adjusting the switching frequency of the converter. A finely controlled zero-current switching (ZCS) scheme together with the accurate MPPT technique enhances the overall efficiency of the converter because of an optimal turn-on time generated by a one-shot pulse generator that is proposed. Moreover, the ZCS technique can deal with low- and high-temperature differences applied to the thermoelectric generator. This allows a wider range of conversion ratios compared to those of conventional converters used for thermal energy harvesting. Experimentally, the converter implemented in a 0.35-μm BCDMOS process had a peak efficiency of 72% at the input voltage of 500 mV while supplying a 5.62-V output.**

***Index Terms*—Battery charger, boost converter, dc–dc converter, energy harvesting, maximum power point tracking (MPPT), one-shot pulse generator, temperature variation, thermal energy harvesting, thermoelectric energy harvesting, thermoelectric generator (TEG), variation.**

I. Introduction

EMERGING energy harvesting devices are being adopted by various applications such as medical sensors, automotive sensors, and smart buildings [1]–[11]. The environmental energy sources for energy harvesting can be solar [1], thermal [2]–[5], vibration [6]–[8], and RF energy [9] as well as wind [10] and even bacteria [11]. Recent works on the thermal energy harvesting convert even body heat into electricity to supply power to electronics devices [2]–[5]. For example, the boost converter in [6] converted a small input voltage of 20 mV to a regulated 1-V output. Low-power control of the converter is achieved by an efficient digital control circuit operating in the discontinuous conduction mode (DCM). The converters in [4] and [12] focused on the start-up issues associated with non-circuit techniques such as the external mechanical switch and the postfabrication process. On the other hand, the converters in [5] and [13] used a transformer for start-up. In most mobile equipment, which necessarily requires a battery, the initial instantaneous high voltage from the battery easily prevents the converter from having start-up difficulties. However, some challenging problems in thermal energy harvesting still need to be overcome in mobile applications. Generally, the output voltage of a thermoelectric generator (TEG) is proportional to the temperature difference ΔT between both sides of the TEG. For example, the temperatures of components, such as the baseband and the transceiver chips popular in cellular phones, may sometimes be increased to more than 70 °C, which will generate a few hundred millivolts at the output of the TEG [14]. In contrast, the normal temperature difference between the two sides of a TEG, body and chips, is only 1–2 °C, which generates just around 50 mV. Therefore, the thermal energy harvesting circuit in some applications such as portable devices should be able to deal with a wide range of TEG output voltages. In this paper, a switching dc–dc boost converter with the high-accuracy zero-current switching (ZCS) control technique for a wide range of conversion ratios is presented. This ZCS technique is realized by a proposed one-shot pulse generator. The maximum power point tracking (MPPT) technique that adjusts the switching frequency of the boost converter according to system variations is also demonstrated. These proposed techniques improve the efficiency of the switching dc–dc boost converter for thermal energy harvesting from 57% to 65% at the input of 100 mV.

This paper is organized as follows. In Section II, the architecture of the proposed thermal energy harvesting system is described. In Section III, the maximum power point (MPP) and variation tracking technique as well as the ZCS scheme for thermal energy harvesting is discussed, and the implementation of the main sub-blocks is described. The measurement results are given in Section IV. Finally, conclusions are presented in Section V.

II. Proposed Thermal Energy Harvesting System

Fig. 1 shows the overall architecture of a power delivery system from a TEG to a power management unit (PMU). Because the voltage generated by the TEG is very small, the start-up of the dc–dc converter must be supported by an instantaneous high voltage from a battery. Fig. 2 shows the timing diagram of the main signals during the start-up operation. While switch S1 is closed during the start-up process, the charge pump CP1 supplies power to the controller of the boost converter. When the oscillator starts to operate, the boost converter starts to convert

Manuscript received March 25, 2012; revised July 5, 2012 and September 27, 2012; accepted November 18, 2012. Date of current version January 18, 2013. This work was supported by the National Research Foundation of Korea Grant funded by the Korea government (MEST) (No. 2011-0020128). Recommended for publication by Associate Editor J. A. Cobos.

The authors are with the Department of Electrical Engineering, Korea University, Seoul 136-701, Korea (e-mail: kjm@kilby.korea.ac.kr; ckim@korea.ac.kr).

Color versions of one or more of the figures in this paper are available online at http://ieeexplore.ieee.org.

Digital Object Identifier 10.1109/TPEL.2012.2231098

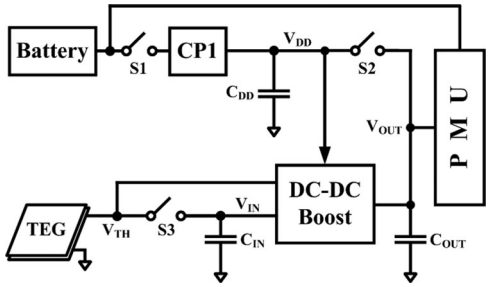

Fig. 1. Architecture of the thermal energy harvesting system.

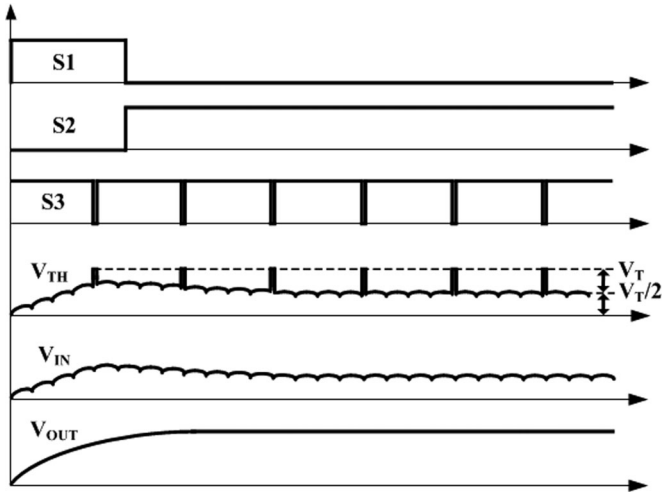

Fig. 2. Timing diagram of main signals during start-up.

the small TEG voltage to a high voltage output for the PMU as well. S1 is then open to cut the power supply from the battery. To avoid chattering, S1 should be opened before the output feedback voltage $V_{\mathrm{OUT\_FB}}$ of the converter reaches the reference voltage V_{REF}. Moreover, by closing switch S2, capacitor C_{DD} is utilized, and the controller of the dc–dc converter is powered by its own output. The input of the converter is periodically disconnected from the TEG by switch S3. To implement the system variation-tolerant MPPT, the open-circuit voltage V_T of the TEG is measured periodically during the short disconnection period. The power loss from this period is negligible because it is very short compared with the connection period. Periodically detaching the TEG from the converter does not affect the operation of the entire system for MPPT, and the converter operates as if it is always connected to S3. The tracking technique for the accurate MPPT is implemented by adjusting the switching frequency of the boost converter. This adjustment process will be explained in the next section.

III. Circuit Implementation

A. Thermoelectric Energy Harvesters

The TEG can be modeled as a voltage source V_T with an internal resistance R_T, where V_T is an open-circuit voltage proportional to the temperature difference between both sides of the TEG and the Seebeck coefficient, as shown in Fig. 3(a). A small R_T means a large power throughput of the TEG. Fig. 3(b) shows

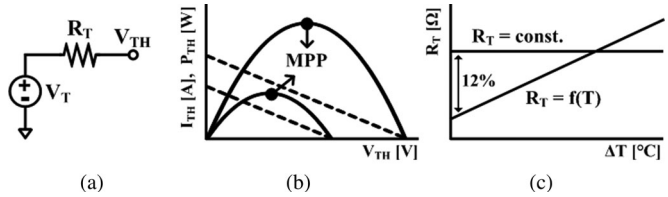

Fig. 3. (a) Electrical equivalent circuit of TEG. (b) Output current I_{TH} versus output voltage V_{TH} (dashed lines) and output power P_{TH} versus V_{TH} (solid curves) of TEG. (c) R_T of TEG versus ΔT.

the output characteristics of a TEG according to two different temperature gradients. The output power from the harvester can reach the MPP at a certain load, and the load impedance corresponds to the input impedance of the converter connected to the TEG. If the load impedance matches R_T, MPPT can be achieved.

In [4], the switching frequency f_{SW} of the converter is determined by R_T of the TEG and the inductor value L. This frequency is used to realize the MPPT for extracting maximum power from the TEG

$$f_{\mathrm{SW}} = \frac{R_T}{8L}. \tag{1}$$

Thus, just setting the frequency to a constant value in (1) activates the MPPT. Unfortunately, this conventional approach has a disadvantage in that it requires the extraction of the exact parameter value (i.e., R_T) of the TEG being used. In addition to the need of accurate TEG modeling, there are several challenging issues with the conventional method. The first problem is that the frequency of general on-chip clock oscillators varies over a wide range depending on process, voltage, and temperature conditions. Second, because R_T of the thermal harvester depends on ΔT, it can deviate by 12% from the design value, as shown in Fig. 3(c) [15]. Finally, in addition to the variation of R_T, a general inductor has an inductance tolerance of at least $\pm 20\%$. Therefore, unless a tracking method is used to deal with these variations, maximum power cannot be obtained from the TEG.

B. Variation-Tolerant MPPT Technique in Thermal Energy Harvesting

The conventional approach for MPPT in thermal energy harvesting uses a switching frequency that is calculated with R_T [4]. However, because this simple technique is affected by variations of many parameters as mentioned previously, the optimal switching frequency needs to be adaptively controlled. Fig. 4 shows the implementation of the proposed converter that realizes the variation-tolerant MPPT by adaptive control of the switching frequency. Because the input voltage V_{IN} of the switching converter has ripples, the average value $V_{\mathrm{TH,AVG}}$ of V_{IN} is obtained using an *RC* low-pass filter. To obtain the maximum power from the thermoelectric harvester, the load impedance should be equal to R_T. In other words, V_{TH} of the TEG needs to be regulated to half of V_T. Based on this MPPT theory, the half value $V_{\mathrm{TH\_HF}}$ of V_{TH2}, which is sensed whenever switch S4 is momentarily closed, is generated by the

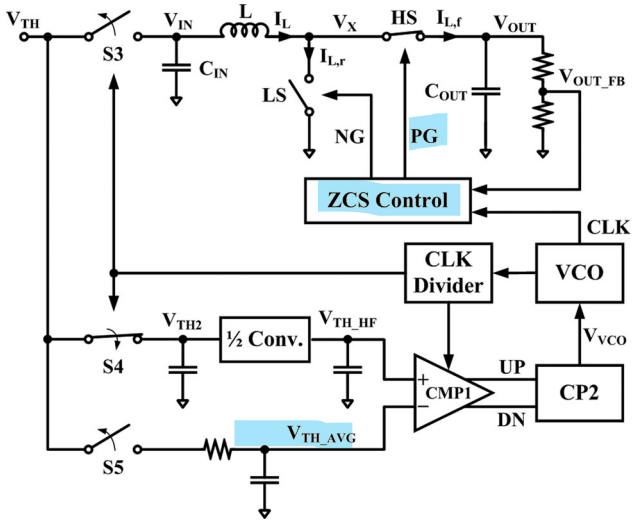

Fig. 4. Block diagram of the proposed dc–dc boost converter with the system variation-tolerant MPPT technique.

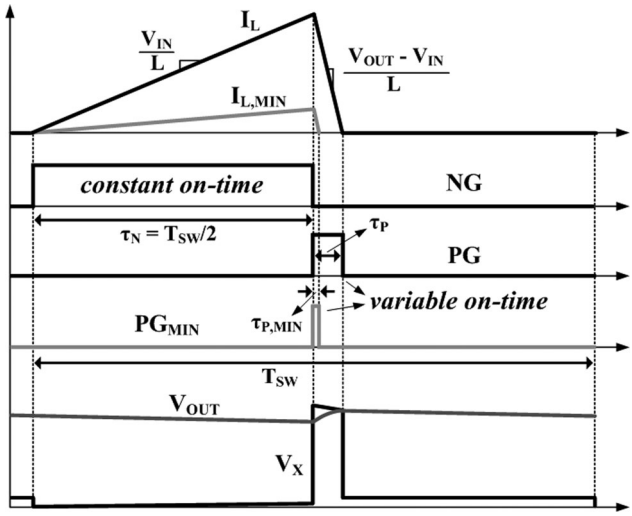

Fig. 5. Theoretical waveforms when the converter operates at the MPP and has an optimal on-time of PG. The subscript MIN means that the input voltage is minimum.

converter with a conversion ratio of 1/2. The on-resistance of S4 has little effect on the accuracy of the MPPT because S4 just transfers the potential from V_{TH} to V_{TH2}. A comparator CMP1 then compares $V_{\mathrm{TH\_HF}}$ to $V_{\mathrm{TH\_AVG}}$. For example, as R_T increases due to the rise of ΔT, V_{IN} decreases to less than half of V_T. To raise the load impedance of the TEG for MPPT, the output signal UP of CMP1 increases the frequency of the output CLK of the voltage-controlled oscillator VCO by controlling the voltage V_{VCO} of the charge pump CP2. Finally, the ZCS control circuit allows the converter to deliver maximum power to the load at the adjusted optimal frequency.

As shown in Fig. 2, the input impedance of the converter is initially set to a high value because of a wrong frequency that resulted from a variation of a system parameter or component value. However, the impedance is adjusted by the tracking process, and V_{IN} is then regulated to half of V_T.

C. ZCS Control for a Wide Range of Input Voltages and the Optimal Turn-On Time

In low-power applications, the continuous conduction mode operation is not efficient because the negative-flowing inductor current cannot be used for power transfer into the converter output [3], [4]. Therefore, the DCM operation which prevents the inductor current from flowing negative is adopted in this design.

While the on-time τ_N of the low-side switch LS in the power stage is set to half of the switching period T_{SW}, the on-time τ_P of the high-side switch HS is finely tuned for the accurate ZCS. Moreover, T_{SW} is decided by (1) and it is controlled for the MPPT, not for tuning τ_P. The clock signal in [3] has a 50% duty cycle, and the converter controls f_{SW} by utilizing pulse-frequency modulation (PFM). This means that the ZCS in [3] controls τ_N. However, our approach is similar to the ZCS control in [4]. In other words, we control τ_P for the ZCS, not τ_N. Therefore, the large quantization error of τ_N that the converter in [3] suffers from can be reduced in this study because τ_P is much smaller than τ_N.

Because the output voltage V_{IN} of the TEG in applications utilizing body heat is very small, $\tau_{P,\mathrm{MIN}}$ is very short like the control signal $\mathrm{PG}_{\mathrm{MIN}}$ of the power stage, as shown in Fig. 5. Thus, the on-time can be controlled just by using the delay of the digital logic gates in the conventional ZCS control circuit [3], [4], [16]. However, the temperature difference across the thermoelectric harvester can become high, so the control signal of HS can have a long duty like the signal PG, as shown in Fig. 5. For example, when the TEG generates 776 mV due to a large temperature difference, the input of the converter needs to be 388 mV at the MPP. In order to convert the input voltage to an output voltage of 5 V with an inductor of 22 μH, HS should be turned ON for 1.48 μs. On the other hand, a very short delay such as 106 ns is used to turn ON HS in the case of a low temperature difference. It is not appropriate to use the gate delay of digital logics to generate such a wide range of falling times of the inductor current I_L since the large area and power consumption as well as high circuit complexity are required. Moreover, the conventional ZCS circuits cannot generate a signal with high resolution on-time to minimize the quantization error, resulting in the high body conduction loss of HS.

Therefore, the logic gates for generating the control signal PG of the switch HS should be replaced with a new one-shot pulse generator. Fig. 6(a) shows the conventional one-shot pulse generator using an RC delay [17]. Once the input pulse IN is triggered, V_{M1} drops to ground potential. Then, the potential of V_{M1} starts to increase while the capacitor C is charged through the resistor R. The time it takes for C to charge to the switching point $V_{\mathrm{INV,SP}}$ of the inverter is $0.7RC$. The output pulse width is defined by this time. This conventional one-shot pulse generator has two limitations; first, the values of both R and C are fixed so the output pulse width cannot be controlled and second, the rate at which the output one-shot pulse is retriggered is limited by the time it takes for V_{M1} to decay back down to V_{DD}. As

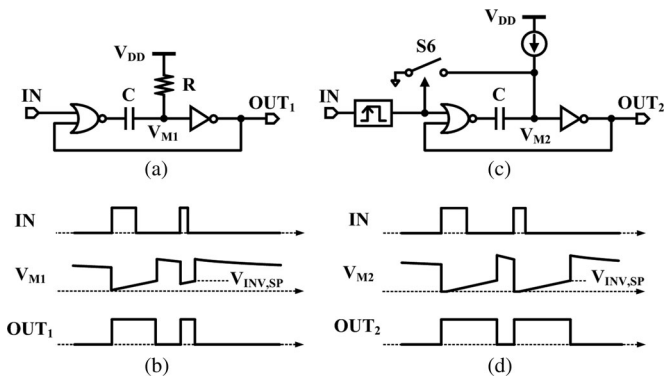

Fig. 6. (a) Conventional one-shot pulse generator and (b) its waveforms. (c) Proposed one-shot pulse generator and (d) its waveforms.

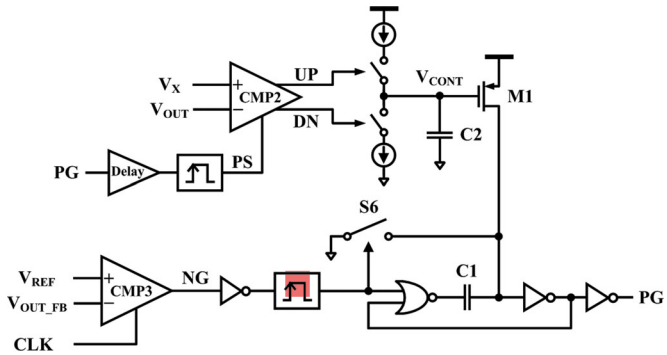

Fig. 7. Proposed ZCS control circuit.

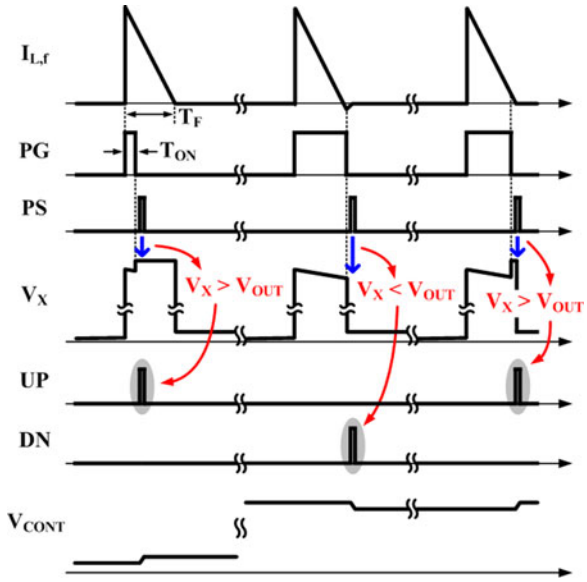

Fig. 8. Timing diagram of the tracking operation for optimum ZCS control.

shown in Fig. 6(b), if the input pulses are close to each other, the output pulses have different widths. This means that the exact pulse width cannot be well defined. Therefore, a one-shot pulse generator is proposed to overcome these constraints, as shown in Fig. 6(c). In order to control the output pulse width, the resistor is replaced with a controllable current source. Controlling the current source allows various pulse widths. Moreover, even though the trigger inputs are close to each other, the output pulse width can be well defined by using a rising-edge detector and a switch. When IN is triggered, the short output pulse of the rising-edge detector closes switch S6, which causes V_{M2} to discharge to ground. Because the initial potential of V_{M2} at which the current source starts to charge the capacitor always becomes zero, the retriggered one-shot can be independent of inputs.

It is indispensable to implement the DCM operation in low-power applications. Therefore, the technique that turns OFF the high-side switch HS once the inductor current crosses zero current is very important. In the conventional implementation of ZCS [18], [19], only a simple comparator is used for the implementation of the DCM, so a comparator offset voltage and a propagation delay of the drivers are produced in the power stage, which result in inaccurate ZCS control and eventual converter efficiency degradation.

Fig. 7 shows the circuit implementation to realize the ZCS control of the inductor current for a wide range of conversion ratios and high-resolution optimal turn-on times. When comparator CMP3 senses that $V_{\mathrm{OUT\_FB}}$ is less than V_{REF}, the inductor starts to be charged for one half of T_{SW}. Then, the inductive energy is transferred to the output through HS. The on-time of this switch should be finely controlled to obtain high converter efficiency. Comparator CMP2 determines whether HS has been turned OFF too early, generating the signal UP, or has been turned OFF too late, generating the signal DN, to achieve optimal ZCS. The output signals of CMP2 finely control the current source M1 by using the output voltage V_{CONT} of the charge pump. The proposed one-shot pulse generator is used in the ZCS control circuit. Therefore, the output signal PG can be defined accurately. The signal PS is a very short pulse, so the current source can be finely controlled. This means that the converter efficiency degradation due to the quantization error from the finite on-time resolution can be minimized. Moreover, the proposed ZCS control circuit allows the current source to produce a very small current. This small and simple circuit enables the output pulse width to be large, while the conventional one-shot pulse generator (or the conventional ZCS circuits) requires a large resistor (or high circuit complexity). This large width means that a wide range of input voltages from the TEG (i.e., big temperature differences) can be applied to the dc–dc converter.

Fig. 8 shows the timing diagram of the tracking operation for optimum ZCS control. $I_{L,f}$ is the falling inductor current flowing through the high-side switch HS of the converter. The gate control signal PG for HS is initially set to zero, and the clock signal PS for comparator CMP2 is a very short pulse triggered a little after PG falls. At this time, if V_X is higher than V_{OUT}, CMP2 outputs UP. Until V_{OUT} increases enough, only UP is continuously generated and V_{CONT} for the current source in the ZCS control circuit is increased, which causes the pulse width of PG to increase. The difference between the inductor current falling time T_F and the PG on-time T_{ON} causes the body conduction loss, which leads to the reduction of the converter efficiency. Finally, once V_X is lower than V_{OUT}, DN at the output of CMP2 is triggered and the inductor reverse current is

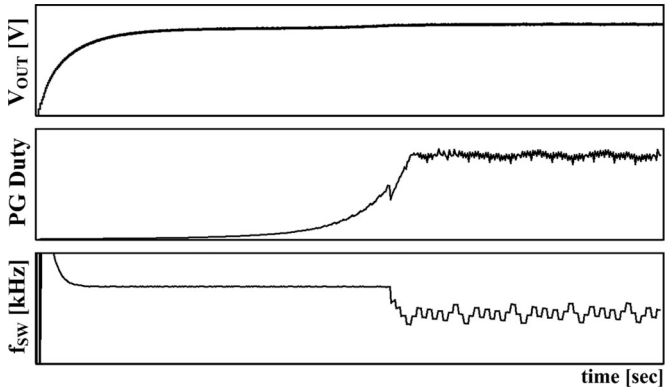

Fig. 9. Simulated waveforms showing tracking of the optimal duty (*Duty*) of the gate control signal PG and the locking for the switching frequency f_{SW}.

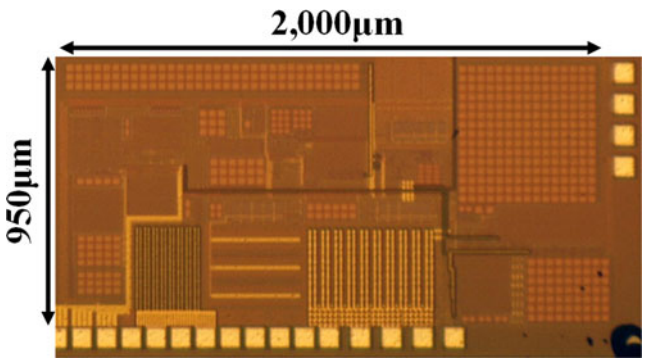

Fig. 10. Chip micrograph.

sensed. To remove this inverse inductor current, the on-time of PG is decreased. Then, UP is triggered again, and both UP and DN alternately occur. Because PS is very short, V_{CONT} can be finely controlled to minimize the body conduction loss due to the limited resolution of PG on-time.

Fig. 9 depicts the simulated waveforms to show the tracking of the optimal duty of PG and the frequency locking for MPPT. The initial switching frequency is fixed by (1) as S1 closes. In the meantime, the duty of HS increases toward the optimal value, and V_{OUT} also increases. S1 is then opened when V_{OUT} increases sufficiently, and then, the frequency tracking starts. Finally, f_{SW} oscillates around the optimal frequency. This optimal frequency is close to the initial value set by (1), which means that the tuning range of the VCO that on average just consumes 50 nW does not affect the overall efficiency of the converter.

IV. Measurement Results

The circuit is implemented in a 0.35-μm BCDMOS process. Fig. 10 shows the photograph of the chip with the boost converter applied with the proposed techniques. The fabricated converter occupies an active area of 1.9 mm^2. The TEG used for the measurement can output 25 mV/K with an internal 8 Ω resistor. The inductor is 22 μH with a parasitic resistance of 120 mΩ. The input capacitor is 10 μF, and the output capacitor is 1 μF.

Fig. 11 shows the measured waveforms that describe the start-up of the proposed converter. The output V_{TH} of the TEG is

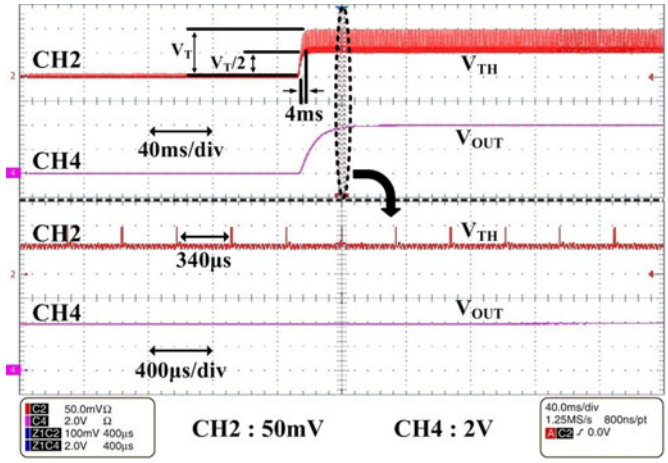

Fig. 11. Measured waveforms of the input and output voltages during start-up operation. The bottom two waveforms show the signals marked with the dotted circle in detail.

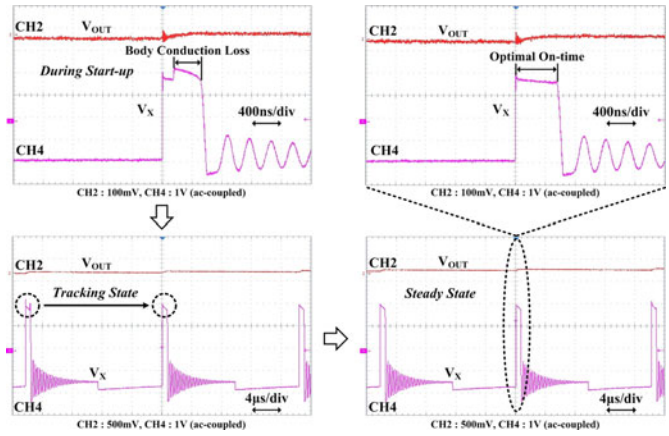

Fig. 12. Measured waveforms describing the tracking of the optimal turn-on time for HS.

periodically disconnected from the input of the converter so that the open-circuit voltage V_T of the TEG can be detected. By adjusting the switching frequency, V_{TH} is regulated to 50 mV, or one half of V_T. This corresponds to a 4 K temperature difference across the TEG. The tracking time of 4 ms is observed. The ripples of the converter input voltage can be observed from the magnified view of the measured waveforms.

The on-time of HS should be the same as the optimal time required to minimize a loss in the converter. As shown in Fig. 9, the initial duty of PG is nearly zero, but the proposed ZCS control circuit enables the duty to reach the optimum value. Fig. 12 shows the tracking process that was carried out for an accurate ZCS of the converter. Because an incorrect on-time causes body conduction loss of the power switch, the ZCS control circuit increases the on-time up to the optimal on-time. Finally, the body conduction loss of HS nearly disappears at the steady state, which is the main contribution to the improvement of the overall efficiency.

Fig. 13 shows the magnified measured waveform of the TEG open-circuit voltage V_T sensed during the short period. V_T (100 mV) of the TEG is sensed for 4 μs, and V_{IN} is regulated to

TABLE I
PERFORMANCE COMPARISON OF STATE-OF-THE-ART WORKS

Parameter	ECT310[21]	Lhermet[2]	Carlson[3]	Ramadass[4]	Im[5]	This work
Process	-	0.35μm	0.13μm	0.35μm	0.13μm	0.35μm
V_{IN} (*: V_T)	20 ~ 500mV*	1V	20 ~ 250mV	25 ~ 100mV*	40 ~ 300mV*	70 ~ 600mV*
V_{OUT}	3 ~ 5V	1.75 ~ 4.3V	1V	1.8V	2V	3~5.8V
Peak Efficiency	30% (just boost converter)	50% (just boost converter)	75% (just boost converter)	58% (end-to-end)	61% (just boost converter)	72.2% (just boost converter)
MPPT	No	No	No	Yes	Yes	Yes
Variation Tolerance	No	No	No	No	No	Yes

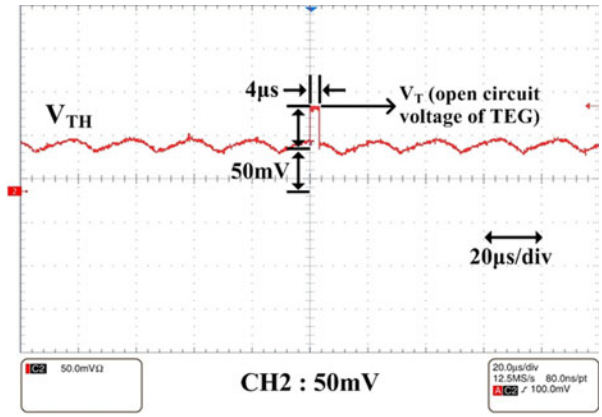

Fig. 13. Magnified measured waveforms for the TEG open-circuit voltage sensed in the short period.

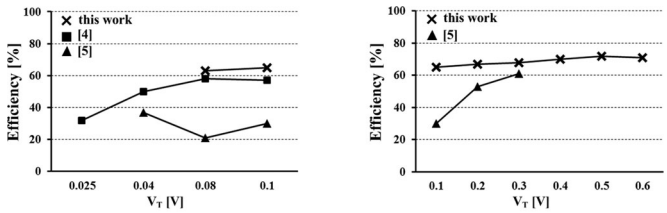

Fig. 14. Efficiency comparison among the latest thermal energy harvesting converters (a) in the low V_T domain and (b) in the high V_T domain.

50 mV, one half of V_T. The short sensing period does not affect the output voltage regulation and rarely degrades the overall efficiency because the sensing interval (340 μs) is relatively long, as shown in Fig. 11. The technique that even eliminates the loss from this short sensing period was recently reported in [5]. However, the converter in [5] suffers from the large power loss due to the transformer used for start-up.

Fig. 14 shows the measured power efficiency curves of state-of-the-art thermoelectric energy harvesting converters as V_T changes. For the efficiency measurement, a load resistor modeling the PMU block in Fig. 1 is connected to the boost converter, and then the output voltage is measured. The input voltage of the PMU block is specified from 3 to 5.8 V in this design. As the load resistance is varied, the output power is measured. As mentioned in [4], the power obtained at the output of the converter is nearly constant under a certain input condition, i.e., V_T, independent of the output conditions. This means that the efficiency can be plotted only according to V_T for efficiency comparison. Fig. 14(a) shows that the efficiency of the proposed circuit at 0.1 V input voltage is 8% greater than that of [4] and 35% greater than that of [5] in the low V_T domain because of the fine control of the duty of HS and the proposed tracking techniques. The power consumption of the control circuitry has little effect on the overall efficiency of our design. The main blocks that consume the static power are the low-dropout linear regulator (LDO) and the bandgap reference (BGR). The LDO consumes about 400 nW and the BGR just consumes 20 nW [20]. The body conduction loss is one of the major losses, but it is reduced by our efficient and accurate ZCS circuit. Fig. 14(b) shows the efficiency of the dc–dc converter in the high input-voltage domain, which cannot be covered by the ZCS control circuit of the conventional converter [4] for thermal energy harvesting. Compared to [5], the proposed techniques also contribute to efficiency improvement in the high V_T domain as well as in the low V_T domain. The efficiency of the obtained output power in the proposed converter reaches 72.2% of the theoretical maximum power available from the TEG with $V_{\rm OUT}$ of 5.62 V and R_L of 5.6 kΩ. At this time, V_T of 500 mV exceeds the input range that can be supported by the converter in [5].

Table I shows the comparison of the performance of the presented converter with those of other switching converters for thermoelectric energy harvesting. The converters in [2], [3], and [21] do not implement the MPPT scheme and are not proper for practical applications. Whereas the control bits for tuning the switching frequency in [4] are manually controlled by external signals, the proposed converter self-tunes the switching frequency for the MPPT. The proposed ZCS circuit supports a wide range of input voltages from the TEG. The finely controlled and accurate ZCS circuit and the variation tracking technique result in the best peak efficiency among converters with the MPPT scheme.

However, the designs in [2], [3], and [5] as well as our study just implement a boost converter, while the energy harvesting architecture in [4] includes two stages of power conversion (storage block for the MPPT and regulation block for the regulation of the output voltage). In our application, the PMU block

regulates the output voltage, as shown in Fig. 1. Because our prototype just implements the dc–dc boost converter and does not includes the PMU block, the converter efficiency obtained would be reduced if a PMU block were to be connected to the boost converter for output regulation. However, the efficiency of the proposed converter would still be competitive with converters with the MPPT scheme [4], [5] if the efficiency of the PMU block were similar to that of the regulation block in [4].

V. Conclusion

A dc–dc boost converter with the variation-tolerant MPPT technique and a high-efficient ZCS control circuit for thermal energy harvesting has been presented in this paper. The MPPT scheme dynamically controls the switching frequency by sensing V_T of the TEG and extracts the maximum power from the TEG. The ZCS control circuit with the proposed one-shot pulse generator finely tracks the optimal time of the falling inductor current to improve the converter efficiency over the conventional coarsely controlled ZCS scheme, which also allows a wide range of conversion ratios.

Acknowledgment

The authors would like to thank the Integrated Circuit Design Education Center for supporting the fabrication through its Multiproject Wafer Program.

References

[1] J. Kim, J. Kim, and C. Kim, "A regulated charge pump with a low-power integrated optimum power point tracking algorithm for indoor solar energy harvesting," *IEEE Trans. Circuits Syst. II, Exp. Briefs*, vol. 58, no. 12, pp. 802–806, Dec. 2011.

[2] H. Lhermet, C. Condemine, M. Plissonnier, R. Salot, P. Audebert, and M. Rosset, "Efficient power management circuit: From thermal energy harvesting to above-IC microbattery energy storage," *IEEE J. Solid-State Circuits*, vol. 43, no. 1, pp. 246–255, Jan. 2008.

[3] E. J. Carlson, K. Strunz, and B. P. Otis, "A 20 mV input boost converter with efficient digital control for thermoelectric energy harvesting," *IEEE J. Solid-State Circuits*, vol. 45, no. 4, pp. 741–750, Apr. 2010.

[4] Y. K. Ramadass and A. P. Chandrakasan, "A batteryless thermoelectric energy-harvesting interface circuit with 35 mV startup voltage," *IEEE J. Solid-State Circuits*, vol. 46, no. 1, pp. 333–341, Jan. 2011.

[5] J.-P. Im, S.-W. Wang, K.-H. Lee, Y.-J. Woo, Y.-S. Yuk, T.-H. Kong, S.-W. Hong, S.-T. Ryu, and G.-H. Cho, "A 40 mV transformer-reuse self-startup boost converter with MPPT control for thermoelectric energy harvesting," in *Proc. IEEE Int. Solid-State Circuits Conf. Dig. Tech. Papers*, Feb. 2012, pp. 104–105.

[6] N. Krihely and S. Ben-Yaakov, "Self-contained resonant rectifier for piezoelectric sources under variable mechanical excitation," *IEEE Trans. Power Electron.*, vol. 26, no. 2, pp. 612–621, Feb. 2011.

[7] Y. Rao and D. P. Arnold, "An input-powered vibrational energy harvesting interface circuit with zero standby power," *IEEE Trans. Power Electron.*, vol. 26, no. 12, pp. 3524–3533, Dec. 2011.

[8] Y. Sun, N. H. Hieu, C.-J. Jeong, and S.-G. Lee, "An integrated high-performance active rectifier for piezoelectric vibration energy harvesting systems," *IEEE Trans. Power Electron.*, vol. 27, no. 2, pp. 623–627, Feb. 2012.

[9] T. Paing, E. A. Falkenstein, R. Zane, and Z. Popovic, "Custom IC for ultralow power RF energy scavenging," *IEEE Trans. Power Electron.*, vol. 26, no. 6, pp. 1620–1626, Jun. 2011.

[10] Y. K. Tan and S. K. Panda, "Optimized wind energy harvesting system using resistance emulator and active rectifier for wireless sensor nodes," *IEEE Trans. Power Electron.*, vol. 26, no. 1, pp. 38–50, Jan. 2011.

[11] A. Meehan, H. Gao, and Z. Lewandowski, "Energy harvesting with microbial fuel cell and power management system," *IEEE Trans. Power Electron.*, vol. 26, no. 1, pp. 176–181, Jan. 2011.

[12] P.-H. Chen, K. Ishida, K. Ikeuchi, X. Zhang, K. Honda, Y. Okuma, Y. Ryu, M. Takamiya, and T. Sakurai, "A 95 mV-startup step-up converter with VTH-tuned oscillator by fixed-charge programming and capacitor pass-on scheme," *Proc. IEEE Int. Solid-State Circuits Conf. Dig. Tech. Papers*, pp. 216–217, Feb. 2011.

[13] "LTC3108: Ultralow voltage step-up converter and power manager," Linear Tech. Corp., Milpitas, CA, 2010 [Online]. Available: http://www.linear.com

[14] "G1-1.0-127-1.27: Tellurex Thermoelectric Energy Harvester," Tellurex, MI, (2007). [Online]. Available: http://www.tellurex.com

[15] A. Mirocha and P. Dziurdzia, "Improved electrothermal model of the thermoelectric generator implemented in SPICE," in *Proc. Int. Conf. Signals Electron. Syst.*, Sep. 2008, pp. 317–320.

[16] Y. K. Ramadass, "Energy processing circuits for low-power applications," Ph.D. dissertation, Massachusetts Inst. Technol., Cambridge, MA, Jun. 2009.

[17] R. Jacob Baker, *CMOS Circuit Design, Layout, and Simulation*. New York: IEEE Press, Wiley-Interscience, 2010, pp. 529–530.

[18] F.-F. Ma, W.-Z. Chen, and J.-C. Wu, "A monolithic current-mode buck converter with advanced control and protection circuits," *IEEE Trans. Power Electron.*, vol. 22, no. 5, pp. 1836–1846, Sep. 2007.

[19] J. A. A. Qahouq, "Control scheme for sensorless operation and detection of CCM and DCM operation modes in synchronous switching power converters," *IEEE Trans. Power Electron.*, vol. 25, no. 10, pp. 2489–2495, Oct. 2010.

[20] L. Magnellij, F. Crupi, P. Corsonello, C. Pace, and G. Iannaccone, "A 2.6 nW, 0.45 V temperature-compensated subthreshold CMOS voltage reference," *IEEE J. Solid-State Circuits*, vol. 46, no. 2, pp. 465–473, Feb. 2011.

[21] "ECT 310 Perpetuum: EnOcean powered by Thermal Energy," EnOcean, Inc., Oberhaching, Germany, 2010 [Online]. Available: http://www.enocean.com

Jungmoon Kim (S'08) received the B.S. degree in electrical engineering from Korea University, Seoul, Korea, in 2007, where he is currently working toward an integrated M.S. and Ph.D. degrees.

His research interests include integrated power management system designs, low-voltage low-power CMOS analog circuit designs, and energy harvesting circuit designs.

Mr. Kim received the Commissioner of Korean Intellectual Property Office Prize at the Korea Integrated Circuit Design Exhibition in 2010, the KEC Analog Design Contest Bronze Award in 2010, and the Chip Design Competition Silver Award at the International Symposium on Integrated Circuits in 2011.

Chulwoo Kim (S'98–M'02–SM'06) received the B.S. and M.S. degrees in electronics engineering from the Korea University, Seoul, Korea, in 1994 and 1996, respectively, and the Ph.D. degree in electrical and computer engineering from the University of Illinois at Urbana-Champaign, Urbana, in 2001.

In 1999, he was a summer intern at the Design Technology at Intel Corporation, Santa Clara, CA. In May 2001, he joined IBM Microelectronics Division, Austin, TX, where he was involved in a cell processor design. Since September 2002, he has been with the Department of Electronics and Computer Engineering, Korea University, where he is currently a Professor. During 2008–2009, he was a Visiting Scholar at the University of California, Los Angeles. His current research interests include wireline transceiver, memory, power management, and data converters.

Dr. Kim received the Samsung HumanTech Thesis Contest Bronze Award in 1996, the ISLPED Low-Power Design Contest Award in 2001, the DAC Student Design Contest Award in 2002, SRC Inventor Recognition Awards in 2002, the Young Scientist Award from the Ministry of Science and Technology of Korea in 2003, the Seoktop Award for excellence in teaching in 2006 and 2011, and the ASP-DAC Best Design Award in 2008. He is currently on the editorial board of IEEE Transactions on Very Large Scale Integration Systems and on the Technical Program Committee of the IEEE International Solid-State Circuits Conference.